Partial-Wave Decomposition of the Ionization Continuum Accessed by Vibrational Autoionization of the NO 14s ($\nu = 1$, $N = 20$, $N_R^+ = 20$) Level

Hongkun Park,* Ian Konen, and Richard N. Zare†

Department of Chemistry, Stanford University, Stanford, California 94305

(Received 2 November 1999)

Rotationally resolved photoelectron angular distributions from vibrational autoionization of the NO 14s ($\nu = 1$, $N = 20$, $N_R^+ = 20$) level are measured by photoelectron spectroscopy, and they are analyzed using a theoretical model based on first-order coupling between the Rydberg level and the ionization continuum. The analysis reveals that λ-changing collisions and l-changing collisions between the molecular-ion core and the outgoing electron are comparable in magnitude and account for 40% of the partial waves produced in the ionization continuum.

PACS numbers: 33.40.+f, 33.60.Cv, 33.80.Eh, 34.50.Gb

In vibrational autoionization of a molecule, the motion of the nuclear framework causes an electron in a high-lying Rydberg state above the ionization limit to escape into the continuum. This process represents a dramatic breakdown of the Born-Oppenheimer approximation that forms the starting point of molecular physics, and as such it has been studied extensively as a test case for our understanding of electron-nuclear coupling [1]. Until now, most of our knowledge on vibrational autoionization has been obtained by analyzing the level structure of high-lying Rydberg levels using multichannel quantum defect theory (MQDT) [2–7]. Despite considerable progress made through these studies, however, a detailed understanding of molecular autoionization events has rarely been accomplished even for a small diatomic molecule owing to the difficulties of probing final quantum states associated with the ion and the photoelectron.

The nitric oxide (NO) molecule has served as a prototypical system for the dynamical study of vibrational autoionization [8–15]. The level-position analyses of the high-lying Rydberg series of NO indicate that the s and d Rydberg series of NO are mixed almost completely to form the s-d Rydberg supercomplexes, whereas the other Rydberg series remain relatively unperturbed [8,9]. The decay dynamics of NO Rydberg states has been shown, on the other hand, to be quite complicated regardless of the electronic orbital angular momentum quantum number l_R because of the interactions between the Rydberg levels and valence electronic states [10–12].

In our previous report of rotationally resolved photoelectron spectra from vibrational autoionization of the NO nl_R ($11 \le n \le 15$, $0 \le l_R \le 3$) Rydberg states, we found that a significant angular momentum exchange takes place between the outgoing electron and the molecular-ion core irrespective of the value of l_R [14,15]. In this Letter, we build on our previous study and report rotationally resolved photoelectron angular distributions (PADs) obtained from vibrational autoionization of the NO 14s ($\nu = 1$, $N = 20$, $N_R^+ = 20$) Rydberg level. To our knowledge, this report represents the first experimental measurement of quantum-state-specific PADs from vibrational autoionization of any molecular system. By fitting experimental PADs to a theoretical model, we obtain a set of dynamical parameters that govern the vibrational autoionization event. These parameters indicate that both dipolar coupling and rotational-electronic coupling between the outgoing electron and the molecular core are important in the vibrational autoionization event, and they are of comparable magnitude. Combined together, they account for approximately 40% of the partial waves produced in the ionization event.

The rotationally resolved PADs from vibrational autoionization of the NO 14s ($\nu = 1$, $N = 20$, $N_R^+ = 20$)

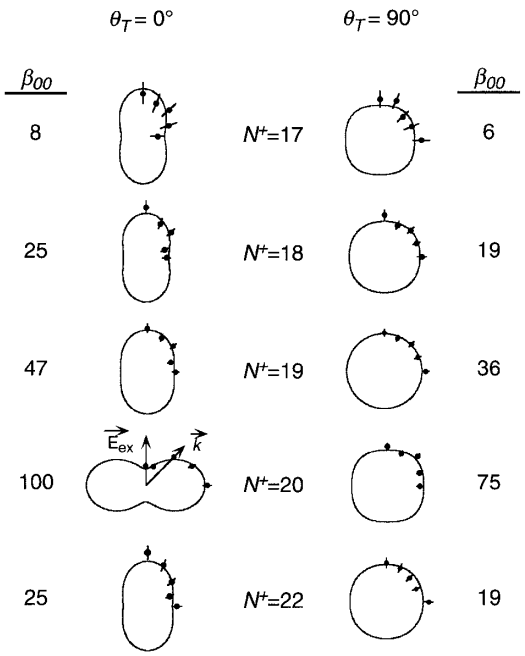

FIG. 1. Polar plots of experimental PADs for five ion rotational levels from vibrational autoionization of the NO 14s ($\nu = 1$, $N = 20$, $N_R^+ = 20$) level. Both the NO 14s-$A\,^2\Sigma^+$ excitation and the NO $A\,^2\Sigma^+$-$X\,^2\Pi$ excitation laser beams are linearly polarized, and θ_T designates the angle between them. The plots are scaled to uniform size. The angle-integrated relative cross sections β_{00} for individual ion rotational levels are listed with PADs. The error bars represent 1σ uncertainties. The solid lines are predictions of the model based on the fit results in Table I.

Rydberg level are measured by combining time-of-flight photoelectron spectroscopy with two-color double-resonance excitation via the NO $A\,^2\Sigma^+$ ($\nu_i = 1$, $J_i = 18.5$, $N_i = 19$) level. A representative photoelectron spectrum obtained from vibrational autoionization of the NO $14s$ ($\nu = 1$, $N = 20$, $N_R^+ = 20$) Rydberg level has been presented in Ref. [15], and the PADs for each ion rotational level are presented in Fig. 1. The PADs are obtained by recording rotationally resolved photoelectron spectra while rotating simultaneously the linear polarization vectors of both excitation laser beams [14–16]. Each PAD in Fig. 1 represents the result of more than 30 000 laser shots per detection angle between the photoelectron propagation direction and the polarization vector of the laser beam that causes the NO $14s$-$A\,^2\Sigma^+$ excitation. The experiment was performed with two different angles held between the polarization directions of two excitation laser beams $\theta_T = 0°$ and $90°$ that produce the same Rydberg level with distinct angular momentum anisotropy [17].

The PADs in Fig. 1 are analyzed using a theoretical model based on first-order coupling between the autoionizing Rydberg level and the ionization continuum. In this model, the photoionization event is treated as a two-step process that consists of the NO $14s$-A-$^2\Sigma^+$ photoexcitation followed by vibrational autoionization of the NO $14s$ ($\nu = 1$, $N = 20$, $N_R^+ = 20$) Rydberg level. The direct photoionization of the NO $A\,^2\Sigma^+$ ($\nu_i = 1$) state to produce the NO^+ $X\,^1\Sigma^+$ ($\nu^+ = 0$) ion and the photoelectron is found to be negligible experimentally, and it is thus ignored [14,15]. In the present model, homogeneous coupling (which preserves the projection of rotational angular momentum onto the molecular axis, λ) between the Rydberg electronic level and the ionization continuum contributes significantly to the vibrational autoionization event [1,18]. Heterogeneous interactions that change λ are included in the model by allowing the coupling matrix elements between the $14s$ Rydberg level and the continuum wave functions with different λ to be nonzero.

The intensity of photoelectrons $I(\theta, \phi)$ detected in the laboratory solid angle element $d\Omega$ can be expressed based on the coupling matrix elements between the Rydberg level and the continuum wave functions as

$$I(\theta,\phi) \propto \sum_{M^+MM'} \langle \mathrm{NO}^+ X\,^1\Sigma^+\ \nu^+ = 0,\ N^+\Lambda^+ = 0M^+;\ \vec{k}'|\hat{\mathbf{H}}_{va}|\mathrm{NO\ Rydberg}\ \nu = 1, NM\rangle \times \langle \mathrm{NO\ Rydberg}\ \nu = 1, NM'|\hat{\mathbf{H}}_{va}|\mathrm{NO}^+\ X\,^1\Sigma^+\ \nu^+ = 0,\ N^+\Lambda^+ = 0M^+;\ \vec{k}'\rangle \rho^N_{MM'}\,. \quad (1)$$

Here, $\hat{\mathbf{H}}_{va}$ represents the Hamiltonian operator responsible for the coupling between the Rydberg level and the continuum wave functions, and $\rho^N_{MM'}$ designates an element of the density matrix for the Rydberg level that specifies the population or coherence between different M sublevels [19]. In Eq. (1), the projection Λ of N onto the molecular axis in the Rydberg level is not specified because the Rydberg level can have different Λ components as a consequence of the Rydberg mixing and the rotational l uncoupling [1].

The matrix elements that appear in Eq. (1) can be expressed in terms of the molecule-frame eigenchannel quantities as [20]

$$\langle \mathrm{NO}^+ X\,^1\Sigma^+\ \nu^+ = 0, N^+0M^+;\ \vec{k}'|\hat{\mathbf{H}}_{va}|\mathrm{NO\ Rydberg}\ \nu = 1, NM\rangle = [(2N^+ + 1)(2N + 1)]^{1/2} \sum_{lm\lambda\alpha_\lambda} (-1)^{m-\lambda} i^{-l} e^{i\sigma_l} \times Y_{lm}(\hat{k}') \begin{pmatrix} N^+ & l & N \\ M^+ & m & -M \end{pmatrix} \begin{pmatrix} N^+ & l & N \\ 0 & \lambda & -\Lambda \end{pmatrix} \times \overline{U}^\lambda_{l\alpha_\lambda} e^{-i\pi\overline{\tau}^\lambda_{\alpha_\lambda}} H_{\alpha_\lambda\lambda}\,, \quad (2)$$

where

$$H_{\alpha_\lambda\lambda} = \langle \nu^+ = 0|\,[\langle \mathrm{NO}^+\ X\,^1\Sigma^+|\,\langle\lambda\alpha_\lambda|\,] \times \hat{\mathrm{A}}\hat{\mathbf{H}}_{va}|\mathrm{NO\ Rydberg}\rangle\,|\nu = 1\rangle\,. \quad (3)$$

The symbols and notations that appear in Eq. (2) follow the conventions in Ref. [20], and $H_{\alpha_\lambda\lambda}$ represents the vibrationally averaged electronic coupling matrix elements between the Rydberg state and the eigenchannel wave function $|\lambda\alpha_\lambda\rangle$. The quantities $\overline{U}^\lambda_{l\alpha_\lambda}$ and $\overline{\tau}^\lambda_{\alpha_\lambda}$ represent the vibrationally averaged eigenchannel mixing coefficients and scattering phase shifts, respectively. In the usual MQDT formulation, the dependence of $U^\lambda_{l\alpha_\lambda}$ and $\tau^\lambda_{\alpha_\lambda}$ on the internuclear distance is responsible for vibrational autoionization [6,21]. In the present model that is based on the first-order perturbation theory, however, the coupling is instead represented by the coupling matrix elements $H_{\alpha_\lambda\lambda}$.

By inserting Eq. (2) into Eq. (1) and by performing integration over all the nonangular coordinates, $I(\theta, \phi)$ can be recast into a familiar form:

$$I(\theta,\phi) = \sum_{L=\mathrm{even}} \sum_{M_L} \beta_{LM_L} Y_{LM_L}(\theta,\phi)\,, \quad (4)$$

in which

$$\beta_{LM_L} = \sum_{lm\lambda} \sum_{l'm'\lambda'} \zeta_{LM_L;N^+lm\lambda l'm'\lambda'} \sum_{\alpha_\lambda\alpha'_\lambda} \overline{U}^\lambda_{l\alpha_\lambda} \overline{U}^{\lambda'}_{l'\alpha'_\lambda} H_{\alpha_\lambda\lambda} H_{\alpha'_\lambda\lambda'} \times \exp[i(\pi\tau^\lambda_{\alpha_\lambda} - \pi\tau^{\lambda'}_{\alpha'_\lambda} + \sigma_l - \sigma_{l'})]\,. \quad (5)$$

Here $\zeta_{LM_L;N^+lm\lambda l'm'\lambda'}$ represents a geometric coefficient that results from angular momentum coupling and the frame rotation, and $H_{\alpha_\lambda\lambda}$, $\overline{U}^\lambda_{l\alpha_\lambda}$, and $\overline{\tau}^\lambda_{\alpha_\lambda}$ constitute the

dynamical parameters that describe the vibrational autoionization process.

The expression in Eq. (4) was used to fit the rotationally resolved PADs presented in Fig. 1 and to extract dynamical parameters, $H_{\alpha_\lambda\lambda}$. The values of $\overline{U}^{\lambda}_{l\alpha_\lambda}$ and $\overline{\tau}^{\lambda}_{\alpha_\lambda}$ were set at the values obtained from previous MQDT analysis of high-lying Rydberg level structures although they can, in principle, be determined from the fit as well [9,15]. As shown previously in the study of direct photoionization of NO $A\,^2\Sigma^+$ and $D\,^2\Sigma^+$ states, the values of $\overline{U}^{\lambda}_{l\alpha_\lambda}$ and $\overline{\tau}^{\lambda}_{\alpha_\lambda}$ determined from Rydberg spectroscopy describe very well the ionization continuum that leads to the NO^+ $X\,^1\Sigma^+$ ($\nu^+ = 0$) ion [22]. In the fit, the partial wave expansion was truncated at $l_{\max} = 3$ and $\lambda_{\max} = 2$. The decision to include σ, π, and δ waves ($\lambda = 0$, 1, and 2, respectively) is based on the λ composition of the NO $14s$ ($\nu = 1$, $N = 20$, $N_R^+ = 20$) Rydberg level determined by a simplified MQDT analysis [15]. The truncation of the partial-wave expansion at $l_{\max} = 3$ is determined, on the other hand, by choosing the minimum number of partial waves that satisfactorily fits the experimental PADs. The inclusion of higher l partial waves (up to $l_{\max} = 5$) did not improve the fit quality while it increased the correlation between fitting parameters significantly. Table I lists the values of $H_{\alpha_\lambda\lambda}$ determined from the fit with the truncation of the partial wave expansion at $l_{\max} = 3$.

The model PADs predicted for each ion rotational level by the dynamical parameters in Table I are shown as solid lines in Fig. 1. The β_{00} values in Fig. 1 designate the angle-integrated relative cross sections for each ion rotational level. As shown clearly in Fig. 1, the parameters given in Table I describe closely the experimental PADs from vibrational autoionization of the NO $14s$ ($\nu = 1$, $N = 20$, $N_R^+ = 20$) Rydberg level. It should be emphasized here that both the angle-integrated relative cross sections as well as the shape of PADs from the fit are in excellent agreement with the experimental data for every ion rotational level. The only parameter randomly adjusted in the fit was the total cross section for the vibrational autoionization process, which could not be determined from the experiment. Although the PADs for ion rotational levels with $N^+ = 21$ and 23 are not shown in Fig. 1 owing to their small cross sections, the fit reproduces β_{00} values for these transitions as well. The fact that the fit correctly reproduces the strong intensity asymmetry between $N^+ = 17$ and $N^+ = 21$ rotational levels is especially remarkable because the marked asymmetry results from distinct interference patterns between the same partial waves [15]. The fact that fit reproduces the asymmetry indicates that the complex interference phenomena between difference partial waves are correctly represented in our fit.

TABLE I. Dynamical parameters that describe the experimental PADs from vibrational autoionization of the $14s$ ($\nu = 1$, $N = 20$, $N_R^+ = 20$) level. The column on the left-hand side represents the values of $H_{\alpha_\lambda\lambda}$ determined from the fit. The values in parentheses represent 1σ uncertainties. The column on the right-hand side presents the values of $\overline{U}^{\lambda}_{l\alpha_\lambda}$ and $\overline{\tau}^{\lambda}_{\alpha_\lambda}$ taken from the MQDT analysis of the spectroscopic data of the high-lying Rydberg series converging to the NO^+ $X\,^1\Sigma^+$ ($\nu^+ = 0$) ion.

Parameter[a]	Fit	Parameter[a]	Value
$H_{sd1,\sigma}$	100(2)	$\overline{\tau}^{\sigma}_{sd2} - \overline{\tau}^{\sigma}_{sd1}$	−1.25
$H_{sd2,\sigma}$	96(2)	$\overline{\tau}^{\pi}_{d} - \overline{\tau}^{\sigma}_{sd1}$	−1.26
$H_{p\sigma}$	80(2)	$\overline{\tau}^{\delta}_{d} - \overline{\tau}^{\sigma}_{sd1}$	1.14
$H_{p\pi}$	44(1)	$\overline{\tau}^{\pi}_{p} - \overline{\tau}^{\sigma}_{p}$	0.06
$H_{d\pi}$	66(9)	$\overline{\tau}^{\sigma}_{f} - \overline{\tau}^{\sigma}_{p}$	−0.65
$H_{d\delta}$	−43(3)	$\overline{\tau}^{\pi}_{f} - \overline{\tau}^{\sigma}_{p}$	−0.65
$H_{f\sigma}$	28(4)	$\overline{\tau}^{\delta}_{f} - \overline{\tau}^{\sigma}_{p}$	−0.65
$H_{f\pi}$	7.1(6)	ϑ^{σ}_{sd}[b]	−0.675
$H_{f\delta}$	28(3)		

[a]The symbols $sd1$ and $sd2$ designate continuum eigenchannels formed by the mixing between $s\sigma$ and $d\sigma$ partial waves. Following the spectroscopic convention, photoelectron partial waves are designated as s, p, d, and f waves for $l = 0$, 1, 2, and 3, respectively.

[b]The matrix elements $\overline{U}^{\lambda}_{l\alpha_\lambda}$ are given by $\overline{U}^{\sigma}_{s,sd1} = \overline{U}^{\sigma}_{d,sd2} = \cos(\theta^{\sigma}_{sd})$ and $\overline{U}^{\sigma}_{s,sd2} = -\overline{U}^{\sigma}_{d,sd1} = -\sin(\theta^{\sigma}_{sd})$; $\overline{U}^{\lambda}_{l\alpha_\lambda} = \delta_{l\alpha_\lambda}$ (for all other l and α_λ).

A simplified MQDT analysis of the Rydberg level positions that includes the interactions between the ns and nd Rydberg manifold indicates that the NO $14s$ ($\nu = 1$, $N = 20$, $N_R^+ = 20$) Rydberg level consists of 79% $s\sigma$, 5% $d\sigma$, and 16% $d\delta$ electronic character [15]. The fit results given in Table I show, on the other hand, that the ionization continuum accessed by the vibrational ionization event has quite different partial-wave composition from the autoionizing level. According to the values of $H_{\alpha_\lambda\lambda}$ in Table I, the $s\sigma$-, $d\sigma$-, and $d\delta$-partial waves still dominate the ionization continuum, contributing approximately 60% to the total ionization cross section. Other partial waves also contribute significantly to the ionization continuum, however, as evidenced by the significant contributions of p and f waves. In addition, the fit results also show that a significant amount of π-partial waves are generated in the ionization continuum despite the small (<1%) π character in the NO $14s$ ($\nu = 1$, $N = 20$, $N_R^+ = 20$) Rydberg level indicated by the simple MQDT analysis. The contribution of π-partial waves is found to be most sensitive to β_{00} values for each ion rotational level and thus rather insensitive to the systematic errors that may be present in experimental PADs. For instance, the large ratio between $\beta_{00}(N^+ = 19)$ and $\beta_{00}(N^+ = 21)$ could not be reproduced by the fit without invoking the $p\pi$-partial waves irrespective of the $l_{\max}$ values for the partial-wave truncation.

The significant contribution of p- and f-partial waves to the ionization continuum indicates that the l-changing collisions between the molecular-ion core and the outgoing photoelectron arise from the dipolar interaction between the ion core and the electron [14,15]. The presence of π-partial waves in the ionization continuum suggests, on the other hand, that the coupling of $\vec{l}$ to the rotation of

the ion core $\vec{N}_R^+$ [1] causes the λ-changing collision to occur between the photoelectron and the molecular ion. The fit in Table I indicates that partial waves produced by the l-changing collisions ($p\sigma$, $f\sigma$, and $f\delta$ waves) and those produced by λ-changing collisions ($p\pi$, $d\pi$, and $f\pi$ waves) contribute almost equally to the ionization continuum, accounting together for approximately 40% of the total ionization cross section. Hence, we reach the conclusion that these two effects, l-changing collisions and λ-changing collisions, are of comparable importance in describing the vibrational autoionization of NO.

As noted previously, the spectroscopic investigations of autoionizing Rydberg states have revealed that the decay dynamics of NO Rydberg states is complicated because of the interactions between the Rydberg and valence electronic states [10–12]. This Rydberg-valence interaction can affect the vibrational autoionization dynamics by mediating the indirect coupling between the Rydberg level and the ionization continuum via the valence electronic state [18]. For the NO $14s$ ($\nu = 1$, $N = 20$, $N_R^+ = 20$) Rydberg level, it has been proposed that the interactions with the $I\,^2\Sigma^+$, $A\,^2\Sigma^+$, and $B'\,^2\Delta$ states are important [12,15]. In this autoionization mechanism mediated by Rydberg-valence coupling, the partial-wave character of the valence states should largely govern the partial-wave character of the outgoing photoelectron. The presence of p- and f-partial waves in the ionization continuum can then be interpreted as a reflection of the electronic character in valence states of NO. The strong presence of the π-wave character in the ionization continuum cannot be explained, on the other hand, based solely on the above homogeneous Rydberg-valence coupling interactions. It requires the heterogeneous interactions between the $14s$ Rydberg level and the Π electronic manifolds through rotational-electronic coupling. This coupling mechanism has been commonly invoked in rotational autoionization but has rarely been discussed in vibrational autoionization. Coupled together, the present findings illustrate that the collisions between the outgoing electron and the molecular core that leads to angular momentum exchange account for the significant portion of partial waves generated in the ionization continuum in vibrational autoionization events. They also suggest that the quantitative MQDT calculations of vibrational autoionization require not only the explicit account for the electron-vibration coupling but also the electron-rotational coupling that includes heterogeneous interactions between different λ manifolds.

This work is supported by National Science Foundation under Grant No. NSF PHY-97-22578.

*Present address: Department of Chemistry and Chemical Biology, Harvard University, 12 Oxford Street, Cambridge, MA 02138.

†To whom correspondence should be addressed.

[1] H. Lefebvre-Brion and R. W. Field, *Perturbations in the Spectra of Diatomic Molecules* (Academic Press, New York, 1986).
[2] G. Herzberg and C. Jungen, J. Mol. Spectrosc. **41**, 425 (1972).
[3] Y. Ono *et al.*, J. Chem. Phys. **73**, 4855 (1980).
[4] C. Bordas *et al.*, Chem. Phys. **129**, 21 (1989).
[5] C. Jungen, S. T. Pratt, and S. C. Ross, J. Phys. Chem. **99**, 1700 (1996).
[6] C. H. Greene and C. Jungen, Adv. At. Mol. Phys. **21**, 51 (1985).
[7] C. Jungen and S. C. Ross, Phys. Rev. A **55**, R2503 (1997).
[8] E. Miescher, Can. J. Phys. **54**, 2074 (1976).
[9] S. Fredin *et al.*, Mol. Phys. **60**, 825 (1987).
[10] Y. Achiba and K. Kimura, Chem. Phys. **129**, 11 (1985).
[11] A. Fujii and N. Morita, Chem. Phys. Lett. **182**, 304 (1991).
[12] S. T. Pratt, J. Chem. Phys. **108**, 7131 (1998).
[13] J. Guo, A. Mank, and J. W. Hepburn, Phys. Rev. Lett. **74**, 3584 (1995).
[14] H. Park, D. J. Leahy, and R. N. Zare, Phys. Rev. Lett. **76**, 1591 (1996).
[15] H. Park and R. N. Zare, J. Chem. Phys. **106**, 2239 (1997).
[16] S. W. Allendorf *et al.*, J. Chem. Phys. **91**, 2216 (1989).
[17] K. L. Reid, D. J. Leahy, and R. N. Zare, J. Chem. Phys. **95**, 1746 (1991).
[18] A. Giusti-Suzor and H. Lefebvre-Brion, Chem. Phys. Lett. **76**, 132 (1980).
[19] K. Blum, *Density Matrix Theory and Applications* (Plenum Press, New York, 1981).
[20] H. Park and R. N. Zare, J. Chem. Phys. **104**, 4554 (1996).
[21] S. Ross and C. Jungen, Phys. Rev. Lett. **59**, 1297 (1987).
[22] H. Park and R. N. Zare, J. Chem. Phys. **104**, 4568 (1996).